Journal of Chemistry

Simulation of Adsorption-Desorption Characteristics of Clay Minerals on Heptadecane: Coupled Grand Canonical Monte Carlo-Molecular Dynamics

Qiuqi Chen[1], Ruigang Zhang[2], Hang Yang[3], Cheng Liu[1,4], Junjie Xiong[1], Zhangping Yan[1], Ruiyu He[1], Linyan Li[1], Xin Tang[1]*

[1]Department of Civil Engineering, Chongqing Three Gorges University, Chongqing, China

[2]Department of Engineering, China University of Mining and Technology, Jiangsu, China

[3]Research Institute of Exploration and Development of Daqing Oilfield Company Ltd. Heilongjiang, China

[4]CNOOC Energy Development Co., Ltd., Tianjin 300452, China

Research Article

Received: 07-Oct-2024, Manuscript No. JCHEM-24-149765; **Accepted:** 21-Oct-2024, PreQC No. JCHEM-24-149765 (PQ); **Published:** 28-Oct-2024.

***For Correspondence:** Xin Tang, Department of Civil Engineering, Chongqing Three Gorges University, Chongqing, China

E-mail: tb15010014b2@cumt.edu.cn

Citation: Chen Q, et al. Simulation of Adsorption-Desorption Characteristics of Clay Minerals on Heptadecane: Coupled Grand Canonical Monte Carlo-Molecular Dynamics.

ABSTRACT

Shale oil is mainly found in nanopores. Clarify the law of shale oil adsorption and occurrence characteristics. It is of great significance to increase domestic crude oil occurrence and production. Based on the Grand Canonical Monte Carlo (GCMC) method, the occurrence model of heptadecane (n-C17) saturated adsorption by illite, montmorillonite and kaolinite was successfully constructed. The saturated adsorption model was also simulated by molecular dynamics. The adsorption pattern and transport process of n-C17 in illite, montmorillonite and kaolinite slits were elucidated. The study shows that there is a difference in the adsorption capacity of different minerals for alkanes. Montmorillonite>illite>kaolinite and the mineral species dominates the isothermal adsorption process. The increase of slit pore size and pressure is helpful to increase the adsorption capacity of clay minerals to n-C17, while the temperature inhibits the adsorption. Under the same temperature and pressure conditions, there was no significant change in the position, thickness and density of the adsorption layer of n-C17. in the micropore to mesopore range. Excess adsorption increases rapidly with increasing pore size, followed by a slow increase. This implies that the percentage of adsorbed state n-C17 decreases gradually with increasing slit pore size. The desorption rate of n-C17 was significantly increased by elevating the temperature under the same pressure condition. The coupled Grand Canonical Monte Carlo-Molecular Dynamics (GCMC-MD) simulation highly restored the adsorption, desorption and transport processes of n-C17 in clay minerals. It describes the occurrence law of alkanes in shale matrix pores and provides a theoretical basis for shale oil exploration and development.

Keywords: Illite; Montmorillonite; Kaolinite; Isothermal adsorption; Density distribution

INTRODUCTION

China's oil shale is mainly distributed in the continental environment and the shale oil reserves are about 4.76 × 1010 t, ranking second in the world. It is an important alternative resource for the country to increase crude oil reserves and production [1-3]. However, shale oil reservoirs are deeply buried and complex in structure, which greatly hinders the exploration and development of shale oil [4-7]. Summarised and compared the advantages and disadvantages of Nuclear Magnetic Resonance (NMR), stepwise pyrolysis and molecular simulation [8-10]. It is pointed out that the molecular simulation technique is able to describe the adsorption behaviour and occurrence state of shale oil in a refined way.

In view of the superiority of molecular simulation technology in describing the molecular force and molecular transport behaviour from the microscopic perspective. Numerous scholars have investigated the mechanism of fluid accumulation in shale nanopores using Monte Carlo method, molecular dynamics and density functional theory [11-16].

Investigated the law of pressure and temperature on the adsorption of alkanes [17]. The adsorption decreases with increasing temperature. Pressure helps to increase the adsorption amount, but the adsorption rate slows down gradually. The author used molecular dynamics combined with Fick's first law to study the transport properties of multicomponent alkanes in shale illite nanopores [18]. The diffusion of alkanes in the confined space satisfies the linear law. The changes of temperature and pressure and pore size are more sensitive to the adsorption of macromolecular alkanes. Constructed pore models for different types of shale [19]. Summarise the effects of pore size, temperature, maturity and driving force conditions on shale oil endowment and explore the shale oil endowment characteristics and flow laws.

Some scholars have studied the effect of shale oil adsorption properties from the perspective of wettability [20-22]. Yu et al., modified inorganic minerals by methylation and hydroxylation [23]. Adsorption simulations were performed for different wetting angle models. Based on drawing isothermal adsorption maps. The contact angle variability of alkane adsorption on mineral surfaces was elucidated from the hydrophilic point of view. The contact angle variability of alkane adsorption on mineral surfaces was elucidated from the hydrophilic point of view. Song et al., constructed a model for the fugacity of n-octane and its mixtures in nanopores [24-26]. The effects of pore size, temperature and pressure, shale oil fraction and wettability on the fugitive state were analysed. Summarise the effects of pore size, temperature, maturity and driving force conditions on shale oil accumulation. Explore the shale oil occurrence characteristics and flow patterns.

Cong et al., combined with previous research results to summarise the adsorption law of alkanes at different temperature and pressure and multi-scale pore size of minerals [27]. The effects of temperature, pressure, pore size and fluid properties on adsorption are shown. However, most scholars use isothermal adsorption simulations to explore the effects of temperature and pressure, mineral type and crude oil fraction on the adsorption law. Simple shale oil storage model is constructed and molecular dynamics simulation is carried out. It is difficult to explore the distribution characteristics and diffusion law of crude oil and to reflect the real shale oil storage state [28-30].

Therefore, based on the temperature and pressure environment under the shale reservoir. The shale oil saturation adsorption model was constructed using GCMC-MD and molecular dynamics simulation was carried out. Reduce the

adsorption law and diffusion characteristics of alkanes in shale minerals under actual geological conditions. Responding to the shale oil in the deep reservoir space.

MATERIALS AND METHODS

Geologic background

The Beibu gulf basin is located in the northwestern part of the South China Sea, adjacent to the Guangdong-Guizhou Rise in the north and the South China Sea Rise in the southeast. The basin has a tectonic layout of two depressions interspersed with one rise, with the Weixinan. Depression being the secondary tectonic unit within the Northern Depression. The lithology of source rocks in Weixinan sag is dominated by semi-deep lake-deep lake facies. Dark gray organic-rich shale, a small amount of mudstone and siltstone are developed. There are many development bands and complex pore structure and a large number of sapropelic type (type I) or humic-sapropelic type (type II) oil shale are developed.

Different studies have shown that the development of nanoscale micropores of clay minerals provides a large specific surface area for shale oil storage. And the pores are mostly filled by organic matter. It is conducive to the transport of hydrocarbons evolved from organic matter to the pore space of clay minerals [31]. X-ray Diffraction (XRD) experiments showed that the main components of shale reservoirs in this area were clay minerals and the content of illite in some sections was as high as 70% (Figure 1).

Figure 1. Saturated hydrocarbon chromatography mass spectrometry of shale oil in Weixinan Sag, Beibu gulf Basin. (a) Shale oil saturated hydrocarbon colour mass spectra; (b) Characteristics of mineral fraction distribution in organic-rich oil shale.

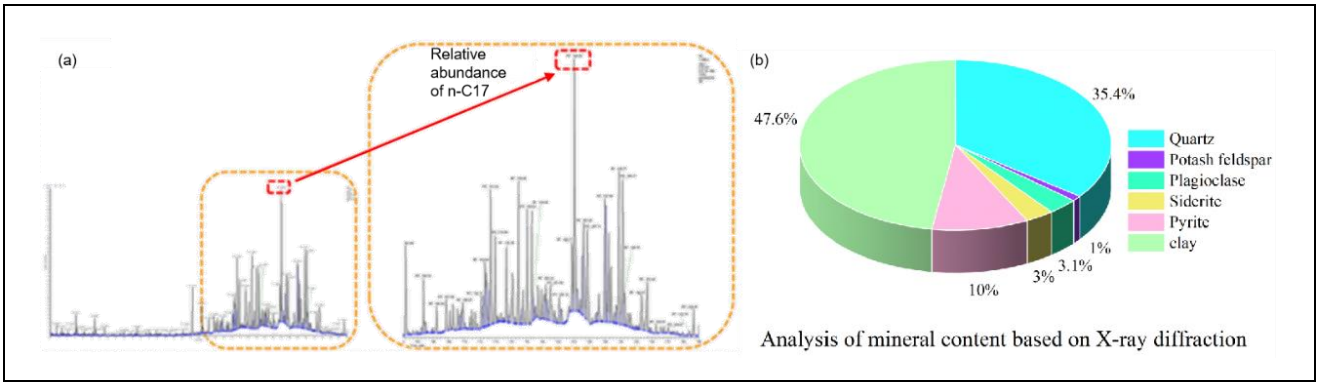

Therefore, the adsorption model of illite with the main component of shale oil is taken as the research object. Molecular dynamics simulation was carried out. Describe the adsorption law and occurrence characteristics of liquid hydrocarbons in clay minerals.

Molecular simulation and analysis methods

Modelling and methodology: Drits et al., experts successfully predicted crystal structure models for illite, montmorillonite and kaolinite based on XRD experiments [32-34]. Ilmenite and montmorillonite are monoclinic crystals with a lattice space group of C2/M. Kaolinite, on the other hand, is triclinic (Table 1). Kaolinite, on the other hand, has a space group of C1 and is a triclinic crystal (Table 1). Similarly, the spatial positions of the atoms of the three clay minerals were also known.

Table 1. Crystal cell parameters of clay minerals.

Mineral type	Space group	a/Å	b/Å	c/Å	α/°	β/°	γ/°
Illite	C2/m	5.2	8.98	10.2	90	101.6	90
Montmorillonite	C2/m	5.23	9.06	12.5	90	99	90
Kaolinite	C1	5.15	8.9	7.38	91.93	105	89.79

The single crystal cell models of illite, montmorillonite and kaolinite were constructed by molecular simulation technology and ion replacement was carried out to ensure charge balance. In the illite octahedron, one of every six Al^{3+} is replaced by Mg^{2+}, while in the Si-O tetrahedron, one of every eight Al^{3+} is replaced by Si^{4+} [35]. Similarly, in the Al-O octahedra of montmorillonite, one out of every eight Al^{3+} is replaced by Mg^{2+} substitution, while in the Si-O tetrahedra, one out of every (Silicon-32) 32 Si^{4+} is replaced by Al^{3+} substitution [36]. Crystals of illite and montmorillonite undergo ionic substitution, where the substitution positions are randomly distributed but not contiguous on the mineral lamellae. The negative charge resulting from the homogeneous substitution is compensated by interlayer cations. The interlayer cations populate the centres of the silica-oxygen tetrahedra at the middle level of the interlayer domains. Based on this, a 4 × 2 × 1 supercell model was expanded from the x, y and z directions. The wall model of the mineral was cut out along the (001) direction. A 4 nm, 8 nm, 15 nm and 50 nm thick vacuum layer was added in the z direction to complete the three clay mineral slit models (Figure 2). Meanwhile, the adsorbent mass model of n-heptadecane was constructed using n-heptadecane as a representative of the heavy component of shale oil [37,38]. Energy optimisation of the slit model and the structure of the n-heptadecane molecule to achieve the lowest energy and stable structure globally.

Figure 2. Construction process of clay mineral slit model. (a) Illite crystal model; (b) Montmorillonite crystal model; (c) Kaolinite crystal model; (d) Structure diagram of heptadecane molecular model.

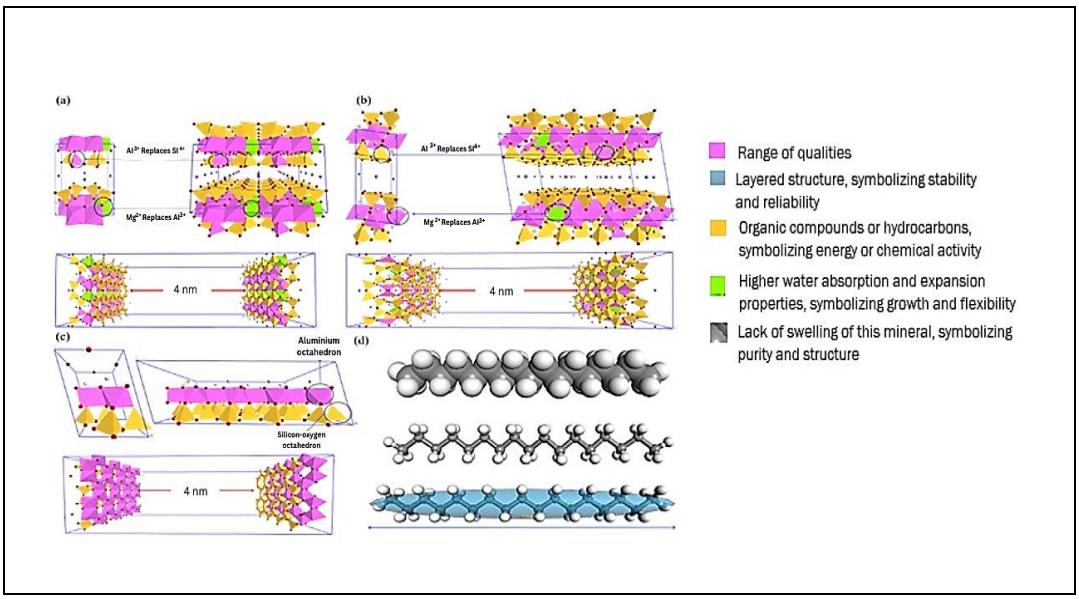

Reduction of a realistic heptadecane molecule (shale oil heavy saturated hydrocarbon fraction, n-C17). Completed modelling of n-C17 fugacity in clay mineral slits. GCMC with molecular dynamics to carry out molecular simulations. Secondly, molecular dynamics simulations were performed on the saturated adsorption model. The density distribution curve of n-C17 was plotted to analyse the adsorption characteristics and distribution law of n-C17. The

molecular dynamics simulation was carried out at a fixed temperature using the Number of particles (N), Volume (V) and Temperature (T) system synthesis. The thermal desorption results of n-C17 at different temperature exercises were investigated. Finally, the desorption rate was calculated by analysing the change of excess adsorption of n-C17 at different pore sizes based on the above simulation results. The transition law of n-C17 fugitive state in the variation of slit pore size of illite, montmorillonite and kaolinite is shown.

The molecular simulations involved in this paper were performed using the Material studio software developed by Accelrys, Inc. which contains the giant regular Monte Carlo method and molecular dynamics theory and has a powerful visualisation interface, which is conducive to the smooth conduct of the study [39].

Simulation process

The optimization of the structure is optimized under the Forcite module. The structural optimization was carried out in the Forcite module. Setting parameters: morphology, structure optimization method is selected as smart and step size is 100000. Adsorption simulation of the optimized model was carried out using Sorption module. The adsorption parameters were obtained from the point-by-point adsorption carried out under the Fixed pressure task. The adsorption method was chosen as Metropolis with an equilibrium step size of 100000 and a total step size of 1000000. A total of three temperature gradient points and 12 pressure points were simulated for the clay reservoir (Table 2).

Table 2. Adsorption simulation temperature and pressure conditions.

Temperature/K	Pressure/MPa											
303.15	0.1	3	5	10	15	20	25	30	35	40	45	50
333.15												
363.15												

Based on this, the occurrence state of n-C17 at 363.15 K and 50 MPa was studied by molecular dynamics. In all the above simulations, the electrostatic and van der Waals forces are calculated by Ewald and Atom based methods and the force fields are chosen from COMPASS [40], which is suitable for organic molecules, small inorganic molecules and covalent molecules of polymers and it has high accuracy in molecular simulation in the field of shale oil research, with the following potential energy functions:

$$E_{totol} = \sum_{bond} E_b(b) + \sum_{angle} E_\theta(\theta) + \sum_{dihedral} E_\phi(\phi) + \sum_{improper} E_x(x) + E_{ele} + E_{vdw} \ldots\ldots(1)$$

where the first five terms represent the energy distribution from the bond, specifically the sum of the energy changes due to bond stretching, bond angle changes, dihedral angle changes, cross terms and off-surface bending potential changes. b, θ, Ø, x, they represent bond length, bond angle, dihedral angle and out-of-plane vibration angle, respectively. The latter two correspond to non-boning interactions, including electrostatic interactions and Vander Waals force interactions, to determine the interactions between particles and help to accurately represent non-bonding interactions.

$$E_{ele} = \sum_{i>j} \frac{q_i q_j}{r_{ij}} \ldots\ldots(2)$$

$$E_{vdw} = \sum \varepsilon_{ij} \left[2\left(\frac{r_{ij}^{\ o}}{r_{ij}} \right)^9 - 3\left(\frac{r_{ij}^{\ o}}{r_{ij}} \right)^6 \right] .....(3)$$

Where r_{ij} is the distance between i and j atoms or molecules. nm; $q_i q_j$ is the charge of atoms i and j; ε_{ij} is the depth of potential well. kJ/mol; r_{ij}^{o} is the distance between atoms i and j in equilibrium, nm.

Calculation method

According to the above settings and boundary conditions, the adsorption capacity of n-C17 in clay mineral slits under different pressures and temperatures was simulated and calculated. The calculation formula is as follows:

$$\mathrm{N} = 1000 \frac{N_{am}}{N_a M_s} .....(4)$$

Where: N is the adsorbed amount in mmol/g; N_{am} is the number of molecules; N_a denotes the number of cells; M_s is the molecular weight of a single cell. The integral method based on density distribution curves is well adapted for determining the density of hydrocarbon adsorbed phases in deep shale nanopores. Therefore, in order to reveal the diffusion pattern of n-C17 in clay minerals. The relative content ratios of adsorbed and free states were clarified. The distribution of n-C17 in the slit pores was finely characterised. Based on the density distribution map, the adsorption region of n-C17 was defined. All n-C17 in this space is endowed in the adsorbed state and the other regions are the endowment space of free n-C17. By integrating and averaging the n-C17 density profiles of the adsorption and free zones and comparing them with the absolute adsorption amount, the adsorption and free state occupancy ratio was obtained [41,42].

RESULTS AND DISCUSSION

Isothermal adsorption

Pressure acts as a driving force in adsorption simulations and molecular dynamics simulations, contributing to the entry of n-C17 into the slit, leading to an increase in absolute adsorption with increasing pressure [43]. However, as the slit pores of the clay minerals were continuously filled with n-C17 (Table 3). The isothermal adsorption curves were mainly divided into three stages, 0.1-5 MPa, 5-40 MPa and 40-50 MPa (Figure 3). They correspond to the rapid growth, slow increase and dynamic equilibrium of n-C17 content with increasing pressure, respectively, which is in agreement with the research results of Zhang et al. [17].

Table 3. Theoretically calculated surface areas of clay minerals.

Mineral type	Molecular formula	Layer spacing/Å	Internal surface area/m²/g	External area/m²/g	Total surface area/ m²/g
Montmorillonite	$Na_{0.75}(Si_{7.75}Al_{0.25})(Al_{3.5}Mg_{0.5})O_{20}(OH)_4$	9.6-21.5	750	50	800
Illite	$Ka_{14}(Si_7AlO_{20})(OH)_4$	10	0	30	30
Kaolinite	$A1_4(Si_4O_{10})(OH)_8$	7.2	0	15	15

Figure 3. The isothermal adsorption diagram of clay minerals on n-C17. (a) 4 nm slit pores; (b) 8 nm slit pores; (c) 15 nm slit pores; (d) 50 nm slit pores.

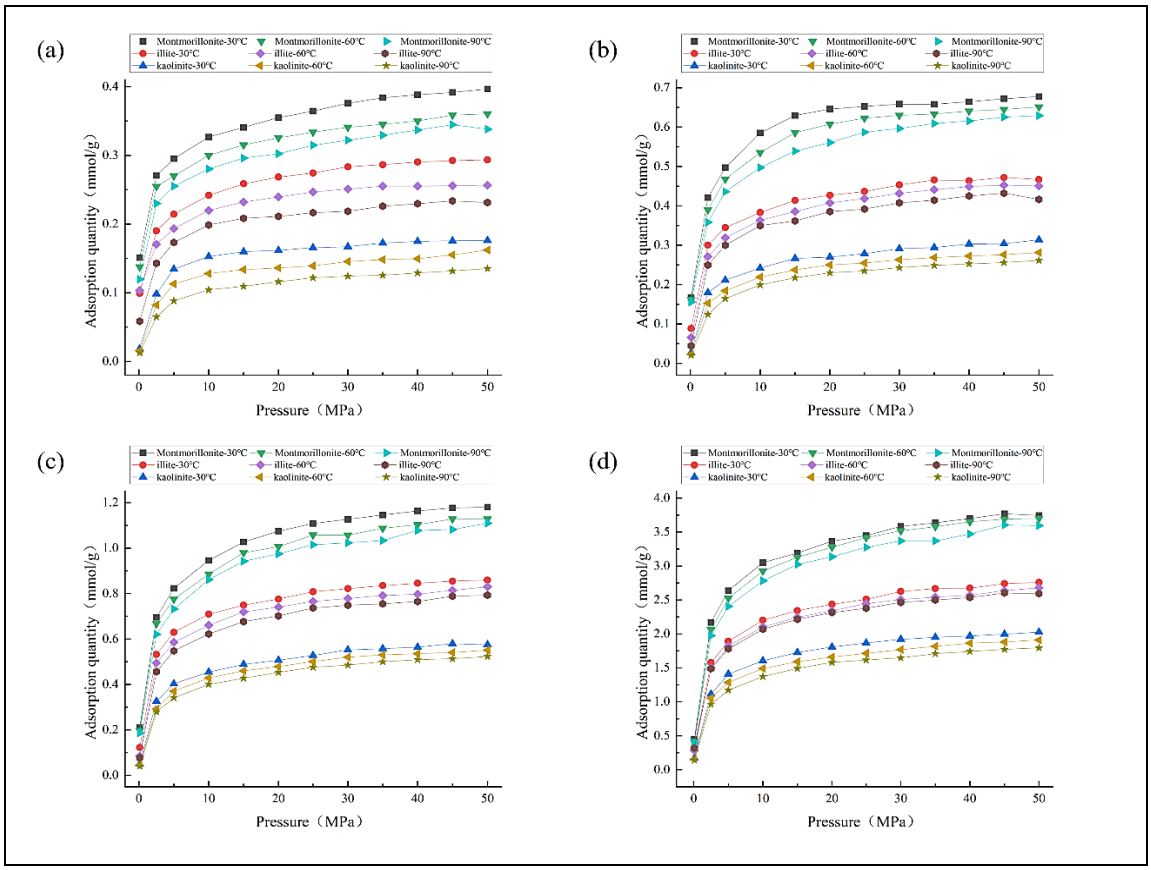

It is obvious that the trends of isothermal adsorption curves of illite, montmorillonite and kaolinite are consistent, but the different clays have obvious boundaries in the amount of n-C17 adsorbed. Under the same temperature and pressure conditions, the trend of adsorption in terms of minerals is: Montmorillonite>illite>kaolinite. The differences in adsorption properties of different clay minerals are mainly due to structural features. Both montmorillonite and illite crystals belong to Tetrahedral-Octahedral-Tetrahedral (TOT) type. Both contain Aluminium-Oxygen Octahedra (O-Al) and Silica-Oxygen Tetrahedra (O-Si) in the lattice structure. The K^+ and Na^+ in the crystal interlayers readily form interactions with the negatively charged portions of the alkanes.

The special configurations and interlayer cations play a key role in the adsorption of alkane molecules, which facilitates the capture of alkanes by the walls [44]. In addition, montmorillonite and illite have a large specific surface area, which provides more adsorption sites for alkane molecules and contributes to the larger n-C17 excess adsorption in the low-pressure phase figure [45,46]. The absolute adsorption in dynamic equilibrium reached saturation adsorption at an adsorption model pressure of 50 MPa. The average increment of montmorillonite to n-C17 adsorption over illite to n-C17 adsorption was 38.6%. The average increment of adsorption of n-C17 by illite over n-C17 adsorption by kaolinite was 55.6%.

At different temperatures, the isothermal adsorption showed regular changes and the adsorption amount of n-17 decreased with the increase of temperature. The effect of temperature on the adsorption process is mainly reflected in the change of energy. Increasing the temperature of the system will radiate the thermal energy to the alkane molecules, so that n-C17 in obtaining energy will be in a high-energy state. Both molecular potential energy and kinetic

energy will be increased to different degrees. The adsorbate in the high kinetic energy state possesses a stronger ability to escape and the Brownian motion is intensified. This leads to the weakening of the interaction between the adsorbed molecules and the mineral surface, making the medium less prone to adsorption.

Analysis of occurrence states

The simulation results show that the absolute amount of adsorption of alkanes by clay minerals and kerogen increases with the enlargement of the slit pore size. This is because there is a positive correlation between the slit pore diameter and the occurrence space of n-C17. In the fugitive space closer to the lamellae, n-C17 is easily captured by the clay minerals due to the van der Waals forces on the walls of the clay mineral slits. An adsorption layer was formed at about 0.86-3.71 nm from the lamellae, with adsorption densities ranging from 0.41-0.56 mmol/g, resulting in a higher density of n-C17 in the adsorption zone. In the fugitive space away from the slit pores, the molecular force of the pore wall on the alkane molecules was significantly reduced, making it difficult to form a high-density adsorption layer.

The n-C17 molecules showed self-aggregation phenomenon and were stored in the slit space in the free state. Due to the large number of data points collected in the molecular dynamics simulation analyses, a large number of burrs appear in the density distribution curves of n-C17 in clay minerals while improving the accuracy. By defining the adsorption and free regions of the alkanes, the proportion of n-C17 assigned in the adsorbed and free states, respectively, was calculated using the integral method (Table 4, Figure 4) [41,42]. It is not difficult to find that there is a large variability in the adsorption properties of clay minerals for n-C17, with montmorillonite>illite>kaolinite.

As the pore size increases, kaolinite, which has a smaller adsorption capacity, will be the first to reach the maximum excess adsorption capacity. Montmorillonite, which has the strongest adsorption capacity, will be the last to reach the maximum excess adsorption capacity. In addition, the modelling of the proportion of different states of n-C17 in clay minerals and its adsorption-freedom conversion showed that the excess adsorption gradually saturated with the increase of pore size, resulting in a gradual decrease in the proportion of adsorbed state n-C17 (Figure 4).

Figure 4. Adsorption-dissociation conversion model of n-C17 in clay minerals. (a) The relationship between the excess adsorption capacity of n-C17 and the pore size of clay minerals; (b) The conversion law between the occurrence state of n-C17 and the pore size of clay minerals.

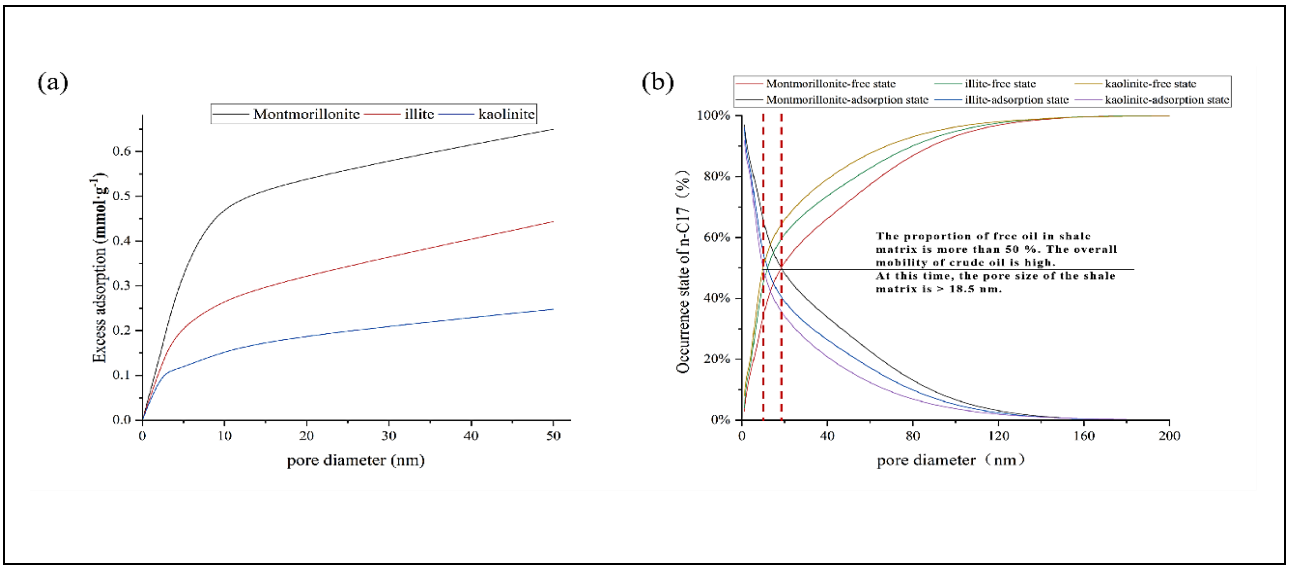

Table 4. The proportion of different occurrence states of n-C17 in clay minerals.

Pore diameter	Mineral type	Adsorption state	Free state
4 nm	Montmorillonite	84.06%	15.94%
	Illite	83.50%	16.50%
	Kaolinite	82.94%	17.06%
8 nm	Montmorillonite	73.09%	26.91%
	Illite	60.16%	39.84%
	Kaolinite	53.86%	46.14%
15 nm	Montmorillonite	47.53%	52.47%
	Illite	38.65%	61.35%
	Kaolinite	34.80%	65.20%
50 nm	Montmorillonite	28.12%	71.88%
	Illite	20.96%	79.04%
	Kaolinite	13.81%	86.19%

The molecular dynamics simulations of high-temperature and low-pressure thermal desorption were completed by increasing the temperatures to 303.15 k, 333.15 k and 363.15 k, respectively, at a pressure of 5 MPa. With the increase of temperature, n-C17 alkane under thermal desorption gradually changed from adsorption state to free state.

The phenomenon of n-C17 alkane moving away from the clay mineral wall appeared and the position of the alkane adsorption layer gradually shifted flat towards the pore centre.

The average displacement of the adsorption centre was 4.01 Å and the average decrease of the peak density distribution was 0.10 g/cm^3. This demonstrated that elevating the temperature favoured n-C17 alkane desorption and by increasing the temperature from 303.15 to 333.15 k at 5 MPa, the n-C17 alkane desorption rate in 4 nm kaolinite was increased from 6.13 to 33.79%, which was much higher than the n-C17 desorption rate in 4 nm montmorillonite (Figures 5-7).

This is due to the temperature, the characteristics of the clay minerals themselves, the pore size and other factors that lead to the phenomenon of inconsistent desorption rate of different clay minerals at different temperatures.

The phenomenon of inconsistency in the travelling distance of n-C17 alkanes in the thermal desorption on the surface of clay minerals exists. In addition, the pores were deformed at high temperatures, which also affected the desorption of n-C17 alkanes on the surface of clay minerals.

Therefore, by elevating the temperature under constant pressure, n-C17ane has desorbability properties and clay minerals with less adsorption are more favourable for n-C17ane desorption (Figure 8).

This provides a new idea for shale oil extraction, using fracturing technology to modify the reservoir pores and enhance the fluidity of hydrocarbons, which is conducive to the increase of crude oil occurrence and production [47]

Figure 5. Adsorption layer displacement of n-C17 in montmorillonite. (a) 4 nm montmorillonite slit density distribution; (b) 15 nm montmorillonite slit density distribution; (c) 35 nm montmorillonite slit density distribution

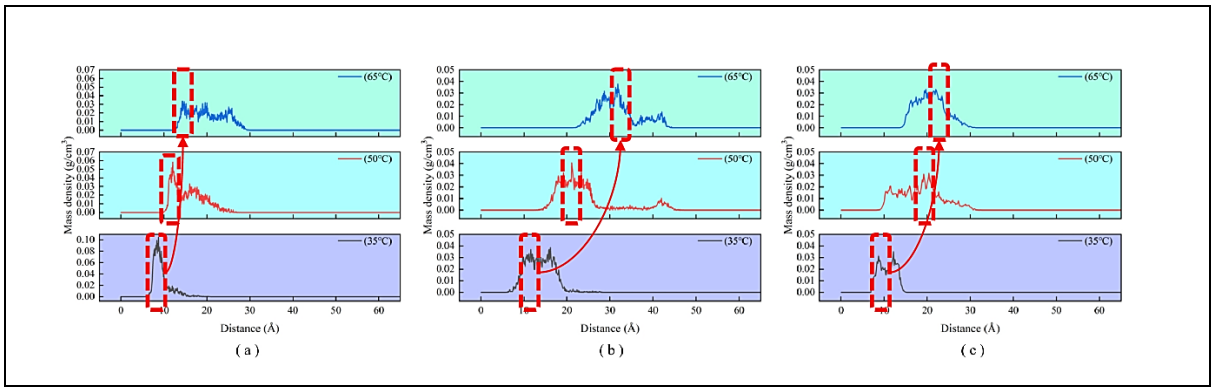

Figure 6. Adsorption layer displacement of n-C17 in kaolinite. (a) 4 nm kaolinite slit density distribution; (b) 15 nm kaolinite slit density distribution; (c) 35 nm kaolinite slit density distribution.

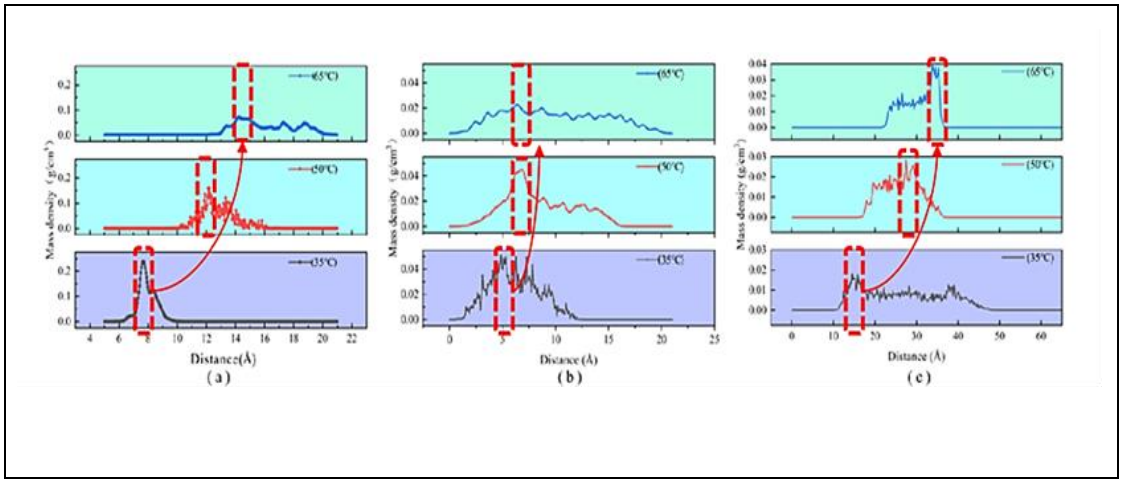

Figure 7. Adsorption layer displacement of n-C17 in illite. (a) 4 nm illite slit density distribution; (b) 15 nm illite slit density distribution; (c) 35 nm illite slit density distribution.

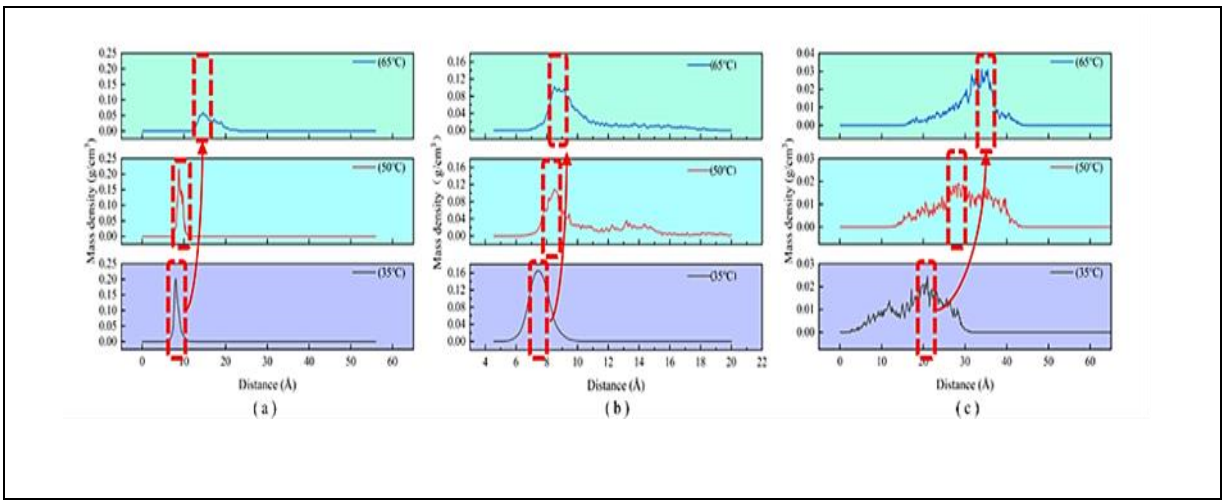

Figure 8. Molecular modelling of adsorption layer displacement of n-C17 in illite. (a) at 303.15 k temperature condition; (b) at 363.15 k temperature condition.

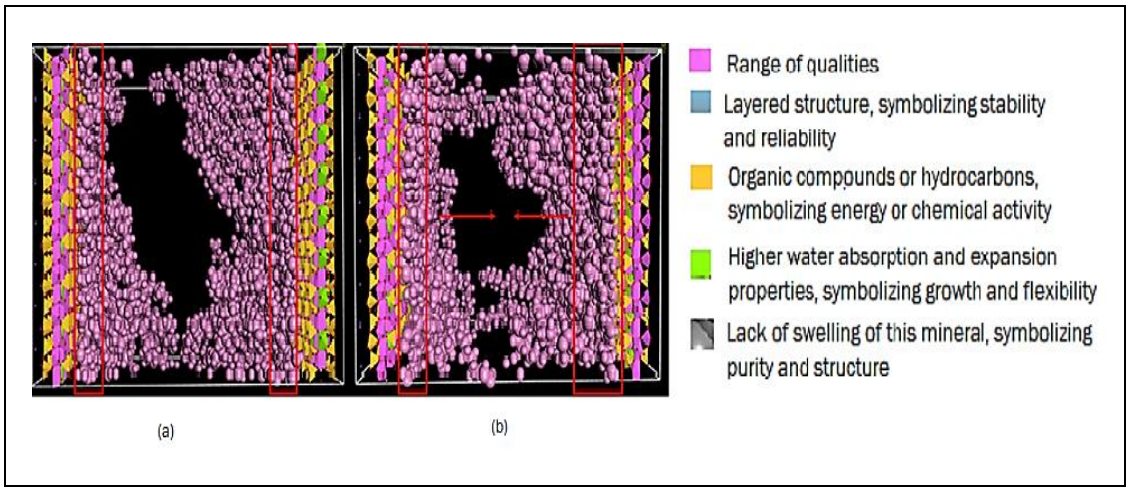

CONCLUSION

Due to the characteristics of mineral crystal structure, the adsorption capacity of different minerals for alkanes is differentiated, with montmorillonite>illite>kaolinite and the mineral species dominating the isothermal adsorption process. In a certain range, the increase of slit size and adsorption pressure contributes to increase the adsorption of n-C17 by clay minerals, while the temperature is unfavourable to the adsorption behaviour of the minerals.Under the same temperature and pressure conditions, the position, thickness and density size of the adsorbed layer of n-C17 did not change significantly. The excess adsorption increased rapidly with increasing pore size in the microporous to mesoporous range, followed by a slow increase. Consequently, the percentage of n-C17 in the adsorbed state decreases gradually with the increase of the slit pore size. Under the same pressure, after elevating the temperature, the position, thickness and density size of the adsorbed layer of n-C17 changed significantly and the transport length satisfied the difference in adsorption energy montmorillonite>illite>kaolinite, the content of n-C17 in the free state was montmorillonite<illite<kaolinite. Based on the coupled GCMC-MD method, we successfully constructed the model of n-C17 fugacity in illite, montmorillonite and kaolinite, which improves the realism of the fugacity state of alkanes in clay minerals. Based on the molecular results of its molecular dynamics simulation, the adsorption-freedom transition model of n-C17 in clay minerals was developed to clarify the evolution of alkane fugacity states at different pore sizes. It helps to understand the shale oil occurrence characteristics in different pore sizes and provides theoretical basis and technical support for the exploration and development of shale oil.

ACKNOWLEDGEMENT

This thesis has been supported by the Key Project of Scientific and Technological Research of Chongqing Municipal Education Commission (Research on Microstructure and Solid-Liquid Adsorption Characteristics of Terrestrial Grainy Shale Oil Reservoir in Chongqing Area, No:KJZD-K202401205), the Youth Project of Chongqing Municipal Education Commission (No: KJQN202401214), Chongqing Engineering Research Center of Disaster Prevention&Control for Banks and Structures in Three Gorges Reservoir Area (No : SXAPGC24YB03), Chongqing Three Gorges University Graduate Research and Innovation Project Funding (No. YJSKY24045), The 2022 Open Fund Project of the National Engineering Research Centre for Offshore Oil and Gas Exploration, characterisation of Oil Shale Microporous Structure

and Study of Crude Oil Mobility' No: (CCL2022RCPS0796RQN), Chongqing Natural Science Foundation of Chongqing, China (No. CSTB2022NSCQ-MSX0333).

REFERENCES

1. Wang Y, et al. Recent techniques on analyses and characterizations of shale gas and oil reservoir. Energy Rep. 2024;3:100067.
2. Bao ST, et al. Geological conditions and reservoir characteristics of various shales in major shale-hosted regions of China. CGS. 2024;7:138-149, 2024.
3. Hu S, et al. Heterogeneous geological conditions and differential enrichment of medium and high maturity continental shale oil in China. Pet Explor Dev. 2022;49:257-271.
4. Guo X, et al. Hydrocarbon accumulation and orderly distribution of whole petroleum system in marine carbonate rocks of Sichuan Basin, SW China. Pet Explor Dev. 2024;51:852-869.
5. Zhao W, et al. Enrichment factors of movable hydrocarbons in lacustrine shale oil and exploration potential of shale oil in Gulong Sag, Songliao Basin, NE China. Pet Explor Dev. 2023;50:520-533.
6. Chen S, et al. Geophysical prediction technology for sweet spots of continental shale oil: A case study of the Lianggaoshan Formation, Sichuan Basin, China. Fuel. 2024.
7. Lei Q, et al. Shale oil and gas exploitation in China: Technical comparison with US and development suggestions. Pet Explor Dev. 2023;50:944-954.
8. Xu L, et al. A review of present research methods on the occurrence of shale oil fluids. Appl Chem Ind. 2024;53:358-367.
9. Li M, et al. Progress of molecular simulation application research in petroleum geochemistry. Oil Gas Geol. 2021;42:919-930.
10. Xue C, et al. Promising combination of CO_2 enhanced oil recovery and CO_2 sequestration in calcite nanoslits: Insights from molecular dynamics simulations. J Mol Liquids. 2023;391:123243.
11. Wu D, et al. The permeability of shale exposed to supercritical carbon dioxide. Sci Rep. 2023;13.
12. Jiang D, et al. Study on the effects of wettability and pressure in shale matrix nanopore imbibition during shut-in process by molecular dynamics simulations. Molecules. 2024;29.
13. Cui J, et al. Molecular simulation of the impact of surface roughness on carbon dioxide adsorption in organic-rich shales. Uncon Resources. 2024;4:100071.
14. Huang T, et al. Molecular simulation of the dynamic distribution of complex oil components in shale nanopores during CO_2-EOR. Chem Eng J. 2024;479:147743.
15. Jin J, et al. Catalytic pyrolysis of oil shale using tailored Cu@zeolite catalyst and molecular dynamic simulation. Energy. 2023;278:127858.
16. Yang S, et al. Comprehensive review: Study on heating rate characteristics and coupling simulation of oil shale pyrolysis. J Anal Appl Pyrolysis. 2024;177:106289.
17. Zhang Y, et al. The effect of salt precipitation on the petrophysical properties and the adsorption capacity of shale matrix based on the porous structure reconstruction. Fuel. 2022;310:122287.
18. Zhang L, et al. Transport property of methane and ethane in K-illite nanopores of shale: Insights from molecular dynamic simulations. Ener Fuels. 2020;34:1710-1719.
19. Chen F, et al. Pore size distributions contributed by various components in the Upper Ordovician Wufeng Shale from Southeast Chongqing, China. J Pet Sci Eng. 2022;208:109230.

20. Xi K, et al. Control of micro-wettability of pore-throat on shale oil occurrence: A case study of laminated shale of Permian Lucaogou Formation in Jimusar Sag, Junggar Basin, NW China. Pet Explor. Dev. 2023;50:334-345.
21. Zhang D, et al. Wettability alteration and slippage effect of adsorbed nanoparticles in tight reservoirs: A molecular simulation. Geo Sci and Eng. 2023;229:212021.
22. Wang F, et al. Molecular dynamics investigation of shale oil occurrence and adsorption in nanopores: Unveiling wettability and influencing factors. Chem Eng J. 2024;481:148380.
23. Yu C, et al. The influence of mineral wettability on the adsorption of shale gas. J-GLOBAL. 2024;41:35-44.
24. Song S, et al. Influencing factors of occurrence state of shale oil based on molecular simulation. Petroleum Reservoir Evaluation and Development. 2023;13:31-38.
25. Xu G. Molecular dynamics numerical simulation of adsorption characteristics and exploitation limits in shale oil microscopic pore spaces. Fluid Dynamics and Materials Processing. 2024;20:1915-1924.
26. Song S, et al. Study on characteristics of shale oil in organic matter pores based on molecular simulation. Energy Chemical Industry. 2022;43:43-49.
27. Cong Q, et al. Review on influencing factors and microscopic mechanism of shale adsorption capacity by molecular dynamics simulation. JCSU (Science and Technology). 2022;53(9):3474-3489.
28. Cong Q. Molecular dynamics simulation of main controlling factors and microscopic mechanism of continental shale gas adsorption. CUP (Beijing). 2023.
29. Wang L, et al. Molecular dynamics analysis on occurrence characteristics of shale oil and competitive adsorption mechanism of CO_2 and oil. JCUP (Edition of Natural Science). 2023;47:128-136.
30. Sun S, et al. A review on shale oil and gas characteristics and molecular dynamics simulation for the fluid behavior in shale pore. J Mol Liq. 2023;376:121507.
31. Huang Y, et al. Logging evaluation of pore structure and reservoir quality in shale oil reservoir: The Fengcheng Formation in Mahu Sag, Junggar Basin, China. Mar Pet Geol. 2023;156:106454.
32. Drits AV, et al. Factors responsible for crystal-chemical variations in the solid solutions from illite to aluminoceladonite and from glauconite to celadonite. Am Min. 2015;95:348-361.
33. Gournis D, et al. A neutron diffraction study of alkali cation migration in montmorillonites. Phys Chem Miner. 2008;35:49-58.
34. Bish DL, et al. Rietveld refinement of non-hydrogen atomic positions in kaolinite. Clays Clay Miner. 1989;37:289-296.
35. Wei P, et al. Nanoscale stick-slip behavior and hydration of hydrated illite clay. Computers and Geotechnics. 2024;166:105976.
36. Liu P, et al. Molecular simulation of the expansion characteristics and hydration mechanism of montmorillonite. World Nuclear Geoscience. 2023;40:598-606.

37. Thoen J, et al. High-resolution and high-accuracy calorimetry of order-disorder and melting transitions in the n-alkanes n-pentadecane, n-hexadecane, n-heptadecane, n-octadecane, n-nonadecane and n-eicosane. The J Chem Thermodyn. 2024;194:107285.

38. Tian S. Micro-pore characteristics of shale reservoirs and evaluation of shale oil occurrence and movability. China University of Petroleum (East China). 2023.

39. Wang Y, et al. Review on the research of different composite coatings. Shandong Chemical Industry. 2019;48:124-125.

40. Rigby D, et al. Computer simulations of poly (ethylene oxide): Force field, PVT diagram and cyclization behaviour. Polymer International. 1997;44:311-330.

41. Liu Y. Fundamental research on the storage characteristics and phase behavior of shale oil and gas. Unconventional Oil and Gas. 2021;8:8-12.

42. Yang Q, et al. Adsorption phase density characteristics of methane in illite pores of deep shale. Fault-Block Oil & Gas Field. 2023;30:799-807.

43. Chen S, et al. Simulation of methane adsorption in diverse organic pores in shale reservoirs with multi-period geological evolution. Int J Coal Sci Technol. 2021;8:1-12.

44. Li T, et al. Insights into the influence mechanism of different interlayer cations on the hydration activity of montmorillonite surface: A DFT calculation. Appl C Sci. 2023;239.

45. Passey QR, et al. From oil-prone source rock to gas-producing shale reservoir-geologic and petrophysical characterization of unconventional shale-gas reservoirs. SPE International Oil and Gas Conference and Exhibition in China. 2010;SPE-131350-MS.

46. Ji L, et al. Experiments on methane adsorption of common clay minerals in shale. Earth Science-Journal of China University of Geosciences. 2012;37(05):1043-1050.

47. Li J, et al. Quantitative evaluation models of adsorbed and free shale oil and its microscopic occurrence mechanism. Oil and Gas Geology. 2019;40:583-592.